Organic–Inorganic Hybrids

Deutsche Ausgabe: DOI: 10.1002/ange.201503661
Internationale Ausgabe: DOI: 10.1002/anie.201503661

Amphiphilic Organic–Inorganic Hybrid Zeotype Aluminosilicate like a Nanoporous Crystallized Langmuir–Blodgett Film**

Takuji Ikeda, Norihito Hiyoshi, Shun-ichi Matsuura, Tetsuya Kodaira, Takuma Nakaoka, Ami Irisa, Miki Kawano, and Katsutoshi Yamamoto**

Abstract: *A new organic–inorganic hybrid zeotype compound with amphiphilic one-dimensional nanopore and aluminosilicate composition was developed. The framework structure is composed of double aluminosilicate layers and 12-ring nanopores; a hydrophilic layer pillared by Q^2 silicon atom species and a lipophilic layer pillared by phenylene groups are alternately stacked, and 12-ring nanopores perpendicularly penetrate the layers. The framework topology looks similar to that of an AFI-type zeolite but possesses a quasi-multidimensional pore structure consisting of a 12-ring channel and intersecting small pores equivalent to 8-rings. The hybrid material with alternately laminated lipophilic and hydrophilic nanospaces can be assumed as a crystallized Langmuir–Blodgett film. It demonstrates microporous adsorption for both hydrophilic and lipophilic adsorptives, and its outer surface tightly adsorbs lysozyme whose molecular size is much larger than its micropore opening. Our results suggest the possibility of designing porous adsorbent with high amphipathicity.*

Zeolite is a key inorganic nanoporous material for a wide range of industrial applications such as ion-exchangers, adsorbents, and catalysts. Its various characteristic properties are strongly related to the crystal structure having highly ordered micropores. Although over 200 kinds of crystal structures of the zeolite are known so far,[1] the demands on zeolites, which have a high potential with regard to catalytic activity, selective adsorption, thermal stability, water/chemical resistance, etc., are continuously increasing. Therefore, in order to give further physicochemical qualities to the framework itself, the development of new zeolitic materials containing various elements as well as functional groups[2] is indispensable. In particular, organic–inorganic hybrid porous solids attract much interest as a new type of functional material, which potentially has unique adsorption ability and high catalytic activity in comparison with conventional zeolites.[3]

The synthesis of organic–inorganic hybrid nanoporous materials has been conducted by a lot of researchers. Tatsumi and co-workers reported ZOL materials with LTA-, MFI-, and *BEA-type zeolite topologies, in which a methylene group bridges two silicon atoms to supersede an oxygen atom in the framework.[4] Also, several covalently linked nanoporous materials having zeolite topology, for example, JUC-Z1[5] (LTA-type) and PSN-1[6] (ACO-type), were synthesized by means of a cross-coupling reaction. Besides, organic–inorganic hybrid porous materials can be prepared from various layered silicates or clay minerals[7–10] and their structures are formed by employing a large bulky organic molecule like an organosilane as a pillar unit in the interlayer space. Recently, Bellussi and co-workers have developed a series of original crystalline aluminosilicates called ECS using a phenylene-bridged bis(triethoxysilyl)benzene (BTEB), some of which showed microporosity.[11]

We also synthesized organic–inorganic hybrid materials using BTEB after these precedents. In our case, however, another silicon source, tetraethyl orthosilicate (TEOS), was used together with BTEB aiming at additional physicochemical properties. A nanoporous crystalline aluminosilicate KCS-2 is one of the materials obtained by this approach,[12] and we have succeeded in solving its crystal structure by powder X-ray diffraction (PXRD) analysis (analysis procedures and crystallographic information are summarized in the Supporting Information (SI); additionally, the structural data can be obtained free of charge from the Fachinformationszentrum Karlsruhe (76344 Eggenstein-Leopoldshafen, Germany; crysdata@fiz-karlsruhe.de) by quoting the depository number CSD-429246). This material turned out to have a sophisticatedly designed structure that can be called a nanoporous crystallized Langmuir–Blodgett film.

The crystal structure of KCS-2 is visualized in Figure 1. From the top view along the *c*-axis (Figure 1 A), zeolite-like 12-ring micropores (effective diameter of 0.74 nm) composed of TO_4 tetrahedra, in which T represents Si or Al, are observed. The hexagonal array of micropores corresponds to that of AFI-type zeolites, as is the case with ECS-14.[11c] From the side view along the *a*-axis (Figure 1 B), an alternate stacking of two aluminosilicate layers is observed; one is a layer pillared with phenylene groups, and the other bridged with Q^2 silicon species ($(-O)_2Si(OH)_2$). The former layer is

[*] Dr. T. Ikeda, Dr. N. Hiyoshi, Dr. S. Matsuura
Research Institute for Chemical Process Technology
National Institute of Advanced Industrial Science and Technology
4-2-1 Nigatake, Miyagino-ku, Sendai 983-8551 (Japan)
E-mail: takuji-ikeda@aist.go.jp
T. Nakaoka, A. Irisa, M. Kawano, Dr. K. Yamamoto
Faculty of Environmental Engineering
The University of Kitakyushu
1-1 Hibikino, Wakamatsu-ku, Kitakyushu 808-0135 (Japan)
E-mail: katz@kitakyu-u.ac.jp
Dr. T. Kodaira
Research Institute for Chemical Process Technology
National Institute of Advanced Industrial Science and Technology
1-1-1 Higashi, Tsukuba 305-8565 (Japan)

[**] This research was financially supported in part by Research Encouragement Grant of The Asahi Glass Foundation.

Supporting information for this article is available on the WWW under http://dx.doi.org/10.1002/anie.201503661.

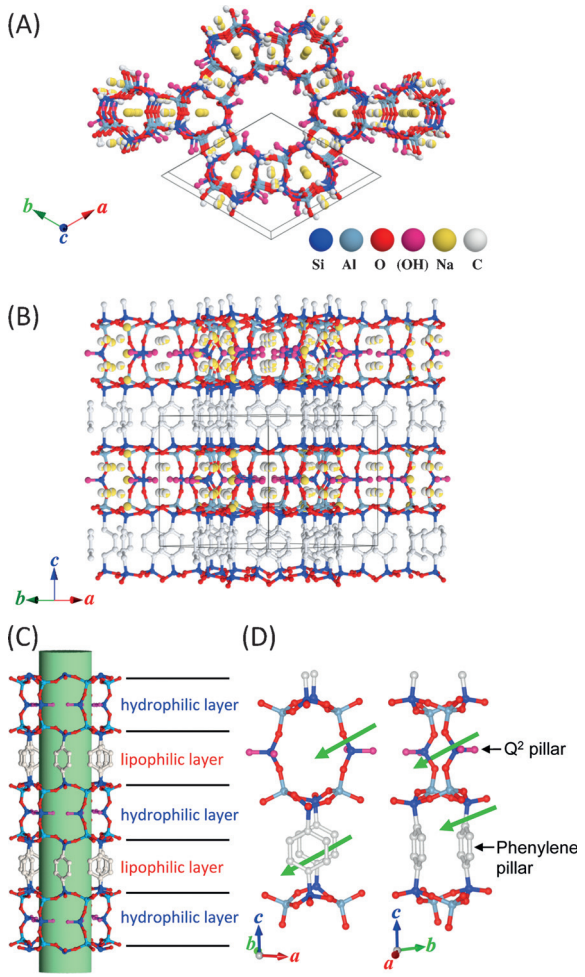

Figure 1. Crystal structure model of KCS-2 determined by PXRD viewed along A) [001] and B) [110] directions. Color balls indicate each constituent element. C) shows the 12-ring straight channel composed of the alternate stacking of hydrophilic layer and lipophilic layer. D) shows two kinds of pillar. In the Q^2 pillar part, ellipse-shaped small pores whose size is equivalent to an 8-ring opening is formed as indicated by the green arrow. A pair of phenylene pillars facing each other forms another ellipsoidal pore opening.

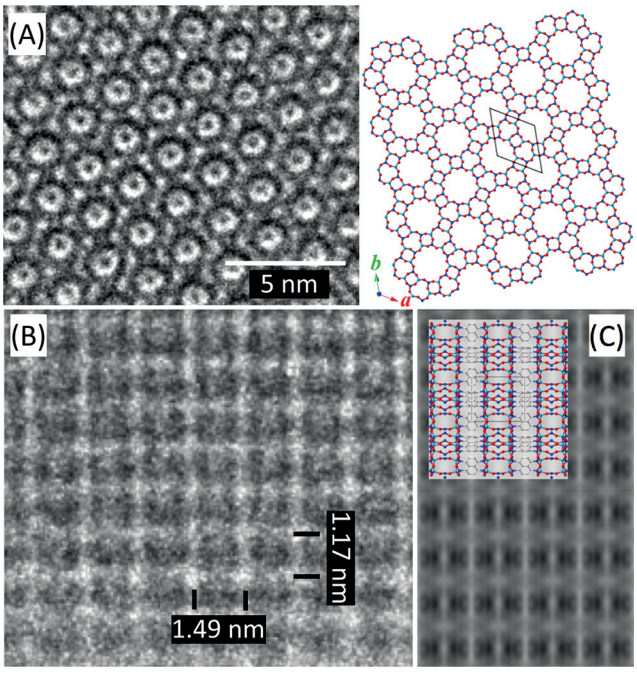

Figure 2. HR-TEM images of KCS-2. A) 12-ring pore channels viewed along the [001] direction and B) side viewed along the [100] direction. C) is a simulated image corresponding to (B) obtained by the multi-slice calculation at a thickness of 7 nm and a defocus length of 80 nm. The lengths of 1.17 nm and 1.49 nm correspond with the $a \times \sin(\pi/3)$ and the lattice constant of the *c*-axis, respectively.

obviously derived from BTEB and also observed in ECS compounds synthesized from BTEB. The latter would be formed owing to the addition of TEOS as a second Si source, and similar layers are observed in Ti-YNU-1[13] bridged with tetrahedral Ti atoms or interlayer-expanded zeolite (IEZ) materials[14–17] bridged with Q^2 silicon species. Surprisingly, in KCS-2, defects of pillars, both Q^2 silicon species and phenylene groups, were hardly observed, that is, all pillar sites were fully occupied. In IEZ materials, the occupancy of Q^2 pillars is only ca. 40–60% in comparison with an ideal model without defects.[16,17] In this way, KCS-2 looks like a "chimera" of the precedent nanoporous materials above, although it is synthesized simply through self-organization.

High-resolution TEM images of KCS-2 evidently support the crystal structure model determined by PXRD analysis. 12-ring straight channels viewed along the [001] direction are arrayed according to hexagonal symmetry (Figure 2A). Incidentally, the morphology of KCS-2 crystallite of a sub-micron size is a hexagonal prism,[12] reflecting this hexagonal symmetry. On the other hand, a grid pattern is observed parallel to the *a*–*c* plane (Figure 2B). The vertical bright lines are attributed to phenylene groups, and the distance between adjacent lines is estimated at ca. 1.49 nm, which coincides with the lattice constant *c*. The completely alternate stacking of two layers is well observed in this actual specimen. Horizontal stripe lines along the [001] direction are arrayed with an interval of 1.17 nm, which almost corresponds to $a \times \sin(\pi/3)$. Figure 2C shows a calculated simulation TEM image along the [100] direction by means of the multislice method. The observed image around the edge of crystal in Figure 2B nicely corresponds to that in the simulated image with the sample thickness of 7 nm.

KCS-2 has straight 12-ring micropores perpendicularly penetrating the stacking layers, which results in the formation of two contrastive nanospaces in one channel. Figure 1C illustrates the cylindrical 12-ring micropore in KCS-2. Within this micropore, a lipophilic nanospace is formed by aluminosilicate layers and phenylene groups facing the inside of the pore wall. Due to the presence of this lipophilic nanospace, KCS-2 shows high absorption capacity for *n*-hexane (1.6 mmol g^{-1}) as shown in Figure 3A. The adsorption isotherm is typical type I, also indicating the strong affinity to organic compounds. It is to be noted that KCS-2 shows far lower adsorption capacity for a bulky 1,3,5-trimethylbenzene. The type II isotherm without a steep step at $P/P_0 = 0$ clearly demonstrates its size-selective adsorption behavior. On the other hand, Q^2 silicon species bridges two aluminosilicate

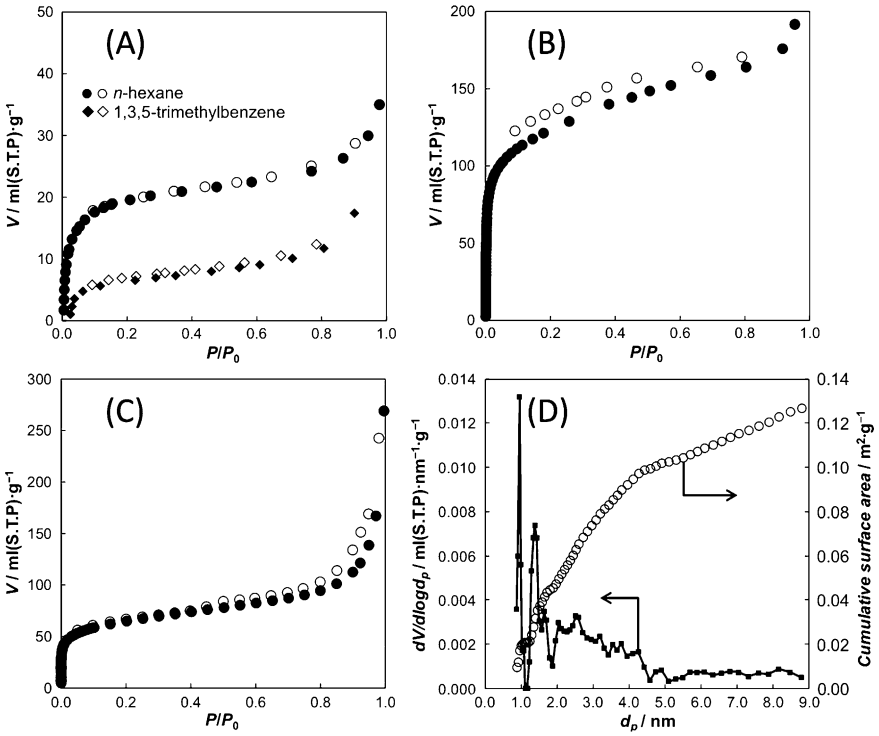

Figure 3. Various gas adsorption isotherms; A) *n*-hexane and 1,3,5-trimethylbenzene at 298 K, B) water vapor at 298 K, C) nitrogen at 77 K, and D) pore size distribution determined by the NLDFT calculation using nitrogen adsorption isotherm.

layers to form another nanospace. A part of silanol groups protrude in 12-ring straight channel, and the presence of these silanol groups makes this interlayer nanospace hydrophilic. N_2 gas adsorption isotherm (Figure 3B) shows a specific surface area of 237 $m^2 g^{-1}$ and a micropore volume, $V(N_2)$, of 0.127 $mL g^{-1}$. It is notable that $V(H_2O)/V(N_2)$, the ratio of adsorbed water volume/micropore volume calculated based on water (Figure 3C) and nitrogen adsorption, of KCS-2 is ca. 1.3 ($V(H_2O) = 0.155$ $mL g^{-1}$), which is comparable with those of typical hydrophilic aluminosilicate zeolites or IEZ analogues.[16,18] This fact indicates the high hydrophilicity of KCS-2. In PXRD structure analysis, three adsorbed H_2O sites were found in 12-ring straight channel, and a large part of the water molecules are distributed in this hydrophilic layer. Also, extraframework Na cations of the quantity equal to framework Al atoms are found in this layer. In this way, two nanospaces having contrasting surface affinities coexist in one straight channel, and consequently KCS-2 exhibits quite a rare amphiphilic surface property. The stacking of lipophilic and hydrophilic layers reminds us of a lamellar phase of surfactants or a lipid bilayer, and it should rather be compared to a "nanoporous crystallized Langmuir–Blodgett film".

It is also to be noted that bridging Q^2 silicon species with aluminosilicate layers is forming an 8-ring opening (0.34 × 0.35 nm). Similarly, pillaring phenylene groups and aluminosilicate layers form a small pore opening (0.31 × 0.45 nm; Figure 1D). Owing to the presence of these openings, complicated inner nanospaces are formed, and both of them are connected with adjacent 12-ring straight channels. Consequently, the micropore system of KCS-2 can be called quasi-three-dimensional. The pore-size distribution based on a nitrogen adsorption measurement showed two kinds of micropores of 0.86 nm and 1.2 nm (Figure 3D). Furthermore, a broad distribution ranging from 2 to 4 nm was observed in Figure 3D, implying the presence of interparticle voids or the formation of interlayer space attributed to the cleavage of the hybrid layered structure.

In addition to the adsorption inside the micropores, the outer surface of KCS-2 crystals showed a characteristic adsorption behavior for an enzyme molecule. The immobilization of enzymes with an inorganic solid has been studied for applications such as drug delivery systems and enzyme catalysts.[19] So far, mesoporous silica with large pore sizes were tested and found to be a suitable support.[20,21] When KCS-2 was used as a support for lysozyme, the adsorbed amount at a low equilibrium concentration was larger than that of SBA-15[22] and nearly equal to that of FSM-16[23] (Figure 4A). Because the molecular size of lysozyme ($3.0 \times 3.0 \times 4.5$ nm)[24] is much larger than the micropore opening of KCS-2, lysozyme molecules would be adsorbed on the outer surface of the KCS-2 crystal as illustrated in Figure 4B. Given that a primary particle of KCS-2 has a diameter of 300 nm and a thickness of 100 nm, it is presumed that the lysozyme molecules densely adhere on the outer surface with the coverage factor of 25–35% (depending on the packing orientation of the molecules) in a closest packing arrangement. This high adsorption capacity would be due to the high hydrophilicity of KCS-2. Even after washing three times with 20 mM Tris-HCl buffer solution (pH 7.5), the immobilized lysozyme did not desorb from KCS-2, indicating a strong affinity between lysozyme and KCS-2.

The solid-state magic-angle nuclear magnetic resonance measurements for ^{27}Al and ^{29}Si nuclei demonstrated the presence of tetrahedral AlO_4, T^3, and Q^2 local environments. The T^3/Q^2 and Si/Al ratios were estimated at 2.0 and 1.5, respectively. These values coincide with those calculated from the structural model above. The empirical Na/Al ratio based on EDX was 1.3, which was larger than the ideal value (1.0) presumably due to the presence of excess Na cation deposited on the crystal surface. A high-temperature PXRD measurement demonstrated that the structure of KCS-2 was stable up to 503 K and desorption of water corresponding to 18.8 wt% was observed until this temperature in a thermogravimetric (TG) measurement. Subsequently a weight loss of 12.7 wt% was observed due to the elimination or combustion of phenylene groups at 503–940 K. Probably, the desorption of water and phenylene groups would occur simultaneously at around 500 K. At higher temperature of > 940 K, a slight

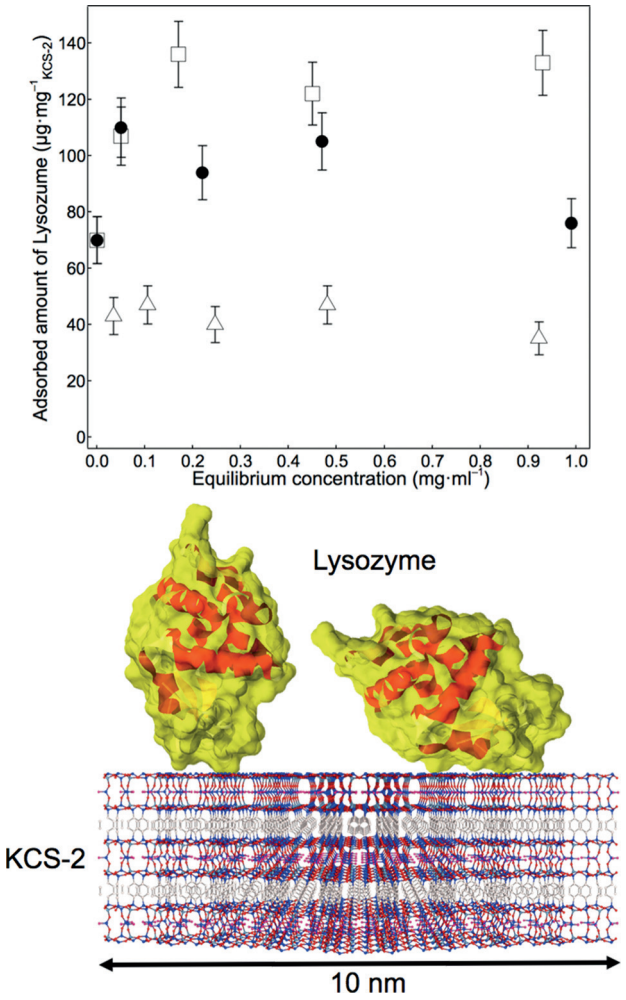

Figure 4. A) Adsorption isotherms of hen egg white (HEW) lysozyme on KCS-2 and mesoporous materials. The amounts of lysozyme adsorbed on KCS-2 (fill circle), FSM-16 (open square), and SBA-15 (open triangle) in 20 mM Tris-HCl buffer solution (pH 7.5) were measured spectrophotometrically with respect to the equilibrium concentrations of lysozyme. B) Illustration of adsorption of HEW lysozyme molecules, whose molecular size is 3.0×3.0×4.5 nm, on the surface of KCS-2.

weight loss of ca. 1.8 wt% was observed, which is due to dehydration–condensation of silanols in Q^2 pillars. From the results above, the chemical composition of KCS-2 is considered to be $|Na_{12}(H_2O)_x|[Si_{18}Al_{12}O_{48}(OH)_{12}(C_6H_4)_6]$, in which x is estimated at 18 for a mildly dehydrated sample and at 32 for a hydrated sample.

Owing to the presence of phenylene pillars, two notable absorption bands were observed at 250–285 nm and 210–235 nm for KCS-2 like ECS-14 by means of diffuse reflectance spectrometry (see SI). The former band was accompanied by three or four fine structures in it. These two bands can be assigned as follows; the lowest photoexcited state of the band at 250–285 nm is based on a π–π* electronic transition of a benzene molecule of the ^1L_b mode in Platt's notation,[25] and the band at 210–235 nm is based on a π–π* electronic transition of a benzene molecule of the ^1L_a mode that has a larger transition dipole moment compared to that of the ^1L_b mode. The fine structures of the π–π* electronic transition of the ^1L_b mode are due to this transition interacting with quantized stretching vibrations of C–H bonding in a benzene ring. The luminescence spectrum excited at 270 nm exhibited a peak at 296 nm, which is higher than those in ECS-14. The peak wavelength of this luminescence was insensitive to the excitation wavelength (see SI). As well as lots of aromatic molecules, the peak of luminescence from KCS-2 appears at longer wavelength than that of absorption, which is usually called the Stokes shift,[26] and the luminescence spectrum has an asymmetric profile with a long tail toward long wavelength direction. Fine structures originating from the interaction between a transition of π*–π and the C–H stretching vibrations should have appeared also on the luminescence spectrum of KCS-2 as well as BTEB in solution (see SI). However, we were able to find no fine structures even if the spectral resolution was narrowed at 1 nm. This indicates that the relaxation from the electronically excited state of aromatic groups in KCS-2 follows a pathway different from that of typical aromatic molecules, for example, anthracene.

Keywords: amphiphiles · Langmuir–Blodgett films · microporous materials · organic–inorganic hybrid composites · zeolite analogues

How to cite: *Angew. Chem. Int. Ed.* **2015**, *54*, 7994–7998
Angew. Chem. **2015**, *127*, 8105–8109

[1] C. Baerlocher, L. B. McCusker, D. H. Olson in *Atlas of Zeolite Framework Types*, *6th ed.*, Elsevier, Amsterdam, **2007**.
[2] C. W. Jones, K. Tsuji, M. E. Davis, *Nature* **1998**, *393*, 52–54.
[3] G. Férey, *Chem. Mater.* **2001**, *13*, 3084–3098.
[4] a) K. Yamamoto, Y. Sakata, Y. Nohara, Y. Takahashi, T. Tatsumi, *Science* **2003**, *300*, 470–472; b) K. Yamamoto, Y. Nohara, Y. Domon, Y. Takahashi, Y. Sakata, J. Plévert, T. Tatsumi, *Chem. Mater.* **2005**, *17*, 3913–3920; c) K. Yamamoto, Y. Sakata, T. Tatsumi, *J. Phys. Chem. B* **2007**, *111*, 12119–12123; d) K. Yamamoto, T. Tatsumi, *Chem. Mater.* **2008**, *20*, 972–980.
[5] Y. Peng, T. Ben, J. Xu, M. Xue, X. Jing, F. Deng, S. Qiu, G. Zhu, *Dalton Trans.* **2011**, *40*, 2720–2724.
[6] W. Chaikittisilp, A. Sugawara, A. Shimojima, T. Okubo, *Chem. Eur. J.* **2010**, *16*, 6006–6014.
[7] R. Ishii, T. Ikeda, T. Itoh, T. Ebina, T. Yokoyama, T. Hanaoka, F. Mizukami, *J. Mater. Chem.* **2006**, *16*, 4035–4043.
[8] A. Corma, U. Díaz, T. García, G. Sastre, A. Velty, *J. Am. Chem. Soc.* **2010**, *132*, 15011–15021.
[9] M. Opanasenko, W. O'Neil Parker, Jr., M. Shamzy, E. Montanari, M. Bellettato, M. Mazur, R. Millini, J. Čejka, *J. Am. Chem. Soc.* **2014**, *136*, 2511–2519.
[10] U. Díaz, A. Corma, *Dalton Trans.* **2014**, *43*, 10292–10316.
[11] a) G. Bellussi, A. Carati, E. D. Paola, R. Millini, W. O. Parker, Jr., C. Rizzo, S. Zanardi, *Microporous Mesoporous Mater.* **2008**, *113*, 252–260; b) G. Bellussi, E. Montanari, E. D. Paola, R. Millini, A. Carati, C. Rizzo, W. O. Parker, Jr., M. Gemmi, E. Mugnaioli, U. Kolb, S. Zanardi, *Angew. Chem. Int. Ed.* **2012**, *51*, 666–669; *Angew. Chem.* **2012**, *124*, 690–693; c) G. Bellussi, R. Millini, E. Montanari, A. Carati, C. Rizzo, W. O. Parker, Jr., G. Cruciani, A. de Angelis, L. Bonoldia, S. Zanardi, *Chem. Commun.* **2012**, *48*, 7356–7358; d) M. Bellettato, L. Bonoldi, G. Cruciani, C. Flego, S. Guidetti, R. Millini, E. Montanari, W. O. Parker, Jr., S. Zanardi, *J. Phys. Chem. C* **2014**, *118*, 7458–7467.
[12] K. Yamamoto, A. Irisa, M. Kawano, T. Ikeda, *Chem. Lett.* **2014**, *43*, 376–378.

[13] W. Fan, P. Wu, S. Namba, T. Tatsumi, *Angew. Chem. Int. Ed.* **2004**, *43*, 236 – 240; *Angew. Chem.* **2004**, *116*, 238 – 242.
[14] S. Inagaki, T. Yokoi, Y. Kubota, T. Tatsumi, *Chem. Commun.* **2007**, 5188 – 5190.
[15] H. Gies, U. Müller, B. Yilmaz, T. Tatsumi, B. Xie, F-S. Xiao, X. Bao, W. Zhang, D. De Vos, *Chem. Mater.* **2011**, *23*, 2545 – 2554.
[16] T. Ikeda, S. Kayamori, Y. Oumi, F. Mizukami, *J. Phys. Chem. C* **2010**, *114*, 3466 – 3476.
[17] J. Jiang, L. Jia, B. Yang, H. Xu, P. Wu, *Chem. Mater.* **2013**, *25*, 4710 – 4718.
[18] T. Yamamoto, Y. H. Kim, B. C. Kim, A. Endo, N. Thongprachan, T. Ohmori, *Chem. Eng. J.* **2012**, *181 – 182*, 443 – 448.
[19] L. Cao, R. D. Schmid in *Carrier-bound Immobilized Enzymes: Principles, Application and Design*, Wiley-VCH, Weinheim, **2005**, p. 1.
[20] S. Hudson, J. Cooney, E. Magner, *Angew. Chem. Int. Ed.* **2008**, *47*, 8582 – 8594; *Angew. Chem.* **2008**, *120*, 8710 – 8723.
[21] C.-H. Lee, T.-S. Lin, C.-Y. Mou, *Nano Today* **2009**, *4*, 165 – 179.
[22] D. Zhao, J. Feng, Q. Huo, N. Melosh, G. H. Fredrickson, B. F. Chmelka, G. D. Stucky, *Science* **1998**, *279*, 548 – 552.
[23] S. Inagaki, Y. Fukushima, K. Kuroda, *J. Chem. Soc. Chem. Commun.* **1993**, 680 – 682.
[24] R. Diamond, *J. Mol. Biol.* **1974**, *82*, 371 – 391.
[25] J. R. Platt, *J. Chem. Phys.* **1949**, *17*, 484 – 495.
[26] T. Nakatsubo, S. Nagasaka, T. Yoshinari, Y. Takahashi, A. Yamamoto, T. Goto, A. Kasuya, *J. Phys. Soc. Jpn.* **2004**, *11*, 3015 – 3019.

Received: April 21, 2015
Published online: May 26, 2015

